HamSCI Personal Space Weather Station: Architecture and Applications to Radio Astronomy

Nathaniel A. Frissell[1*] Scott H. Cowling[2] Thomas C. McDermott[2]
John Ackermann[2] Dave Typinski[3] William Engelke[4] David R. Larsen[2]
David G. McGaw[5] Hyomin Kim[6] David Witten[2] Julius M. Madey[2]
Kristina V. Collins[7] John Gibbons[7] David Kazdan[7] Aidan Montare[7]
Dev Raj Joshi[1] Veronica I. Romanek[1] Cuong D. Nguyen[1] Steve Cerwin[8]
William Liles[8] Jonathan D. Rizzo[8] Ethan S. Miller[8] Juha Vierinen[9]
Philip J. Erickson[10] Mary Lou West[11]

[1]The University of Scranton, Scranton, Pennsylvania
[2]Tucson Amateur Packet Radio (TAPR), Tucson, Arizona
[3]AJ4CO Observatory, High Springs, Florida
[4]The University of Alabama, Tuscaloosa, Alabama
[5]Dartmouth College, Hanover, New Hampshire
[6]New Jersey Institute of Technology, Newark, New Jersey
[7]Case Western Reserve University, Cleveland, Ohio
[8]Ham Radio Science Citizen Investigation (HamSCI) Community
[9]The University of Tromsø, Tromsø, Norway
[10]MIT Haystack Observatory, Westford, Massachusetts
[11]Montclair State University, Montclair, New Jersey (Emerita)

Abstract

The Ham Radio Science Citizen Investigation (HamSCI) Personal Space Weather Station (PSWS) project is a citizen science initiative to develop a new modular set of ground-based instrumentation for the purpose of studying the structure and dynamics of the terrestrial ionosphere, as well as the larger, coupled geospace system. PSWS system instrumentation includes radio receivers sensitive to frequencies ranging from the very low frequency (VLF) through very high frequency (VHF) bands, a Global Navigation Satellite System (GNSS) receiver to provide Total Electron Content (TEC) measurements and serve as a precision time and frequency reference, and a ground magnetometer sensitive to ionospheric and geospace currents. Although the PSWS is designed primarily for space weather and space science, its modular and open design in both hardware and software allows for a variety of use cases. The core radio instrument of the PSWS, the TangerineSDR, is a wideband, direct sampling 100 kHz to 60 MHz field programmable gate array (FPGA)-based software defined radio (SDR) receiver with direct applicability to radio astronomy. In this paper, we describe the PSWS and TangerineSDR architecture, show examples of how the TangerineSDR could be used to observe Jovian decametric emission, and discuss the applicability of the TangerineSDR to radio astronomy in general.

*nathaniel.frissell@scranton.edu

Contents

1 Introduction

The ability to advance the state of knowledge in the fields of radio astronomy and space science is increasingly dependent on the ability to acquire and process large amounts of high-quality, broadband radio spectrum measurements from numerous receivers, potentially spread across a large geographical domain. These types of measurements could enable advancements that range from improved characterization of S-burst Jovian decametric emissions to better understanding the dynamics and causes of short temporal, large spatial scale ionospheric variability. Recent technological advances in the fields of radio engineering, computing, precision timing, and networking have created the potential to make this type of data acquisition and processing accessible even to amateur scientists.

Software Defined Radio (SDR) technology is at the heart of making these measurements. SDRs work by digitizing signals as early in the receiver as possible, then using digital signal processing (DSP) techniques to filter, analyze, demodulate, and otherwise process the signal. This has tremendous advantages over traditional, analog techniques in that SDRs are not limited to a single, predefined signal processing scheme. Even so, all SDRs ultimately have hardware components and design choices that limit their abilities. This becomes apparent when searching for SDRs for use in radio astronomy or space science applications, which often have requirements (i.e., Dodd et al., 2019) that are at odds with communications applications. For instance, HF communications receivers typically use narrow bandwidths and automatic gain control (AGC). They have little need for precision timestamping ($\lesssim 100$ ns), precision frequency measurement (better than parts in 10^{-10}), or calibrated amplitude measurements. Furthermore, communications receivers often obscure access to raw measurements and low-level controls. While SDR-based communications receivers may be inexpensive due to market competition and economies of scale, radio scientists are forced to either reduce their requirements or purchase significantly more expensive, specialized hardware to meet their needs.

In response, the Ham Radio Science Citizen Investigation (HamSCI, http://hamsci.org) and the Tucson Amateur Packet Radio Corporation (TAPR, http://tapr.org) have teamed up to develop a new, modular SDR architecture known as the TangerineSDR that could address the specific needs of a scientific investigator while equally serving other applications (Cowling, 2020). This effort falls under the larger umbrella of the HamSCI Personal Space Weather Station (PSWS) project, which arose out of an interest from the amateur radio community to better understand ionospheric radio wave propagation and a United States National Science Foundation (NSF) Atmospheric and Geospace Science (AGS) Section program to develop new Distributed Array of Small Instruments (DASI) for the advancement of Space Science. This work builds on earlier efforts of Frissell et al. (2014, 2018, 2019) to use amateur radio observations for ionospheric sounding, and is leading to the creation of global amateur radio networks carefully designed for space weather/space science applications (Collins et al., 2021a,b).

Although the HamSCI PSWS and TangerineSDR are initially being developed with Ionospheric and Space Science applications in mind, the open and modular design of TangerineSDR makes it a particularly attractive choice for numerous radio astronomy applications. In this paper, we describe the purpose and architecture of the HamSCI PSWS (Section 2), the architecture of the TangerineSDR (Section 3), examples of radio astronomy applications of the TangerineSDR (Section 4), and additional radio astronomy considerations with respect to the TangerineSDR (Section 5). A summary is presented in Section 6.

2 HamSCI Personal Space Weather Station

2.1 PSWS Purpose

The HamSCI Personal Space Weather Station (PSWS) is designed to be a modular, multi-instrument, ground-based device to observe space weather effects both as a single-point measurement and as part of a larger, distributed network. The PSWS aims to support two primary groups of users: space scientists and amateur radio operators. Each of these groups have different but related needs. For instance, space science researchers need to observe, characterize, and understand ionospheric variability across a range of spatial and temporal scales, understand the coupling between the neutral atmosphere, ionosphere, and magnetosphere, and validate and improve models with the goals of prediction and understanding. Meanwhile, amateur radio operators seek to understand and predict radio propagation to support amateur radio communications, including public and emergency service operations, contesting, and long distance (a.k.a. DX) communications.

Amateurs often also want to study space weather and propagation for personal edification and to contribute back to science and the radio art.

HF ionospheric refraction enables long-distance, over-the-horizon radio communications (of interest to radio operators) while simultaneously providing a mechanism for ionospheric remote sensing (of interest to scientists). This type of radio wave propagation is illustrated in Figure 1 using 2D numerical raytracing through a model ionosphere from the WWV transmitter near Fort Collins, Colorado (blue diamond) to the W2NAF receiver in Spring Brook Township, Pennsylvania (red star). The top raytrace shows computed ray paths for a 15 MHz radio wave along the WWV-W2NAF path, while the bottom shows paths for a 10 MHz wave. The red path indicates the ray that links the transmitter to the receiver. Background colors represent plasma frequency, which can be directly related to ionospheric electron density with the relation $f_p \approx 9\sqrt{N}$, where f_p is the plasma frequency in Hz and N is the electron density in m^{-3}. Both raytraces were computed using the PHaRLAP raytracing toolkit (Cervera and Harris, 2014; Coleman, 1998) with the International Reference Ionosphere 2016 (IRI2016) empirical model (Bilitza et al., 2017).

It is important to note several features in the raytraces shown in Figure 1. First, the ray path that connects the transmitter to the receiver passes through, and hence will be modulated by, the ionosphere. This is the primary feature that enables remote sensing. Second, the amount of refraction is a function of both ionospheric density and frequency. In Figure 1, the densities are the same in the top and bottom figure, but the radio frequency is not. It is apparent that the high frequency (15 MHz) wave undergoes less refraction than the lower frequency (10 MHz) wave. This dispersion is the reason it is important to collect signals spread throughout the HF band when trying to diagnose the ionospheric state. Third, not all rays remain trapped between the Earth and ionosphere. If rays exceed a critical takeoff angle and/or a critical frequency, they will escape into space. This is bad for communications, but good for radio astronomers who are trying to sense signals from outside of Earth. It is important to remember how the ionosphere varies spatially and temporally. Ionospheric production is predominantly driven by photoionization, and there are strong diurnal, seasonal, and solar cycle dependencies. Additionally, the actual ionosphere is not smooth as shown in the IRI model. Instead, it can be highly variable and structured.

With this in mind, it can be said that the primary purpose of the PSWS is to receive as many signals-of-opportunity on the HF bands as possible and apply the physics illustrated in Figure 1 in order to understand the ionospheric state and dynamics. This is why the core instrument of the PSWS is the radio instrument, as described in Section 2.2 below.

2.2 PSWS Architecture

The HamSCI PSWS comes in two primary flavors: the low-cost "Grape" PSWS (US ∼\$300), and the performance-driven "TangerineSDR" PSWS (US ∼\$500 – \$1000). The radio instrument in the Grape PSWS is a purpose-built receiver specifically for observing ionospherically-imposed Doppler shifts on high frequency signals and therefore has limited utility in the field of radio astronomy. Instructions for building a Grape Version 1 are available at http://hamsci.org/grape1 and by Gibbons et al. (2021). Conversely, the TangerineSDR PSWS is designed to be an extremely flexible, precision radio instrument with numerous potential radio astronomy applications.

Figure 2 shows the standard block diagram for the TangerineSDR-based HamSCI PSWS. In this version, the PSWS has three main instruments: the general-purpose software defined radio (SDR), the Global Navigation Satellite System (GNSS) / Global Positioning System (GPS) Receiver, and the ground magnetometer. The heart of the PSWS is the SDR, which provides raw spectrum data from ∼100 kHz to 60 MHz that can be simultaneously processed into multiple data products. The GNSS receiver serves multiple purposes. First, it provides precision time and frequency references for the entire PSWS system. Secondly, it is an ionospheric instrument in its own right, capable of providing ionospheric total electron content (TEC) and scintillation measurements. Finally, the ground magnetometer is used to sense perturbations in the Earth's magnetic field due to currents in the ionosphere and space. The SDR and GNSS receiver functions will be handled by the TangerineSDR, whose architecture is described in more detail in Section 3. The ground magnetometer board will utilize a low-cost 3-axis PNI RM3100 magnetometer module with a ∼10 nT field resolution. Details of the ground magnetometer are given by Madey et al. (2021) and Kim et al. (2021). In addition to the three primary instruments described above, the modular design allows for the addition of future instruments, such as the very low frequency (VLF) receiver described by Rizzo (2021). Conversely, any one of the instruments shown may be used separately from the others.

All of the PSWS instrumentation will be tied together by a central computer running the PSWS Local Host Software. This computer will provide a local user display, local user data reduction, and communicate with the central control and database server. On basic installations of the PSWS, this computer will likely be a single-board computer such as a Raspberry Pi, but users with greater requirements may substitute a more powerful computer. Data processing will be shared between the field-programmable gate array (FPGA)-based SDR and the general purpose computer as most appropriate. Data will be uploaded via the internet to a publicly accessible database to allow for coordinated analysis. The central server will also be able to send updates and issue commands to control PSWS nodes in the network. It is noted that the HamSCI PSWS system is an open-source system, and node owners retain full control of their station. Therefore, the uploading of data and participation in the centrally-controlled system is voluntary. Furthermore, users will be given reasonable methods of accessing the most basic data products produced by the system, as well as methods for loading their own analysis code. Details of the PSWS control software and database are given by Engelke (2021, 2020).

3 TangerineSDR

The TangerineSDR system consists of two main components (see Figure 3). The component on the left, and the focus of this section, is a three or four board modular stack consisting of a Data Engine (DE) carrier board, a Clock Module (CKM) and one or two RF Modules (RFM). On the right, a Single Board Computer (SBC) or other general-purpose computer acts as the host, providing networking, protocol formatting, and other functions. The TangerineSDR uses a modular design to allow users to select the feature set required for their specific use case. Details of TangerineSDR architecture and philosophy were first published by Cowling (2020).

3.1 Data Engine

The block diagram of the Data Engine, or DE, is shown in Figure 4. The DE is the heart of the radio portion of the TangerineSDR and offers two sockets for RF Modules (RFM) as well as a single socket for a Clock Module (CKM). Low data-rate instruments (such the ground magnetometer or VLF module) and Raspberry Pi HATs can be connected through the Low-speed Expansion Adapter Fixture (LEAF) interface. At the center of the DE is an Intel MAX10 FPGA. This FPGA receives and processes the digitized RF data streams from the two RFMs. The resultant processed data is then sent out over either USB 3.0 or gigabit Ethernet to the host or other destination determined by the host. Data processing can be simple packetization, frequency mixing, decimation, filtering, formatting of data, and/or many other possibilities. For the PSWS, the FPGA will split the incoming broadband data stream into multiple narrow-band streams (called virtual receivers) that are sent out as UDP-streamed packets over gigabit Ethernet. Virtual receivers can be up to 20 MHz wide or more (typical width is 192 kHz) and can be independently set to any center frequency between 100 kHz and 60 MHz; the DE can create a number of these (typically a maximum of 8 to 16). The width and number of virtual receivers is limited by the bandwidth of the gigabit Ethernet interface to an aggregate bandwidth of 20 to 30 MHz.

3.2 Clock Module

The Clock Module, or CKM, is the key component that allows for precision frequency measurement and timestamping. Figure 5 shows the block diagram of the CKM. The CKM has an on-board multi-band Global Navigation Satellite System (GNSS) receiver enabling ionospheric total electron content (TEC) and scintillation measurements, as well as providing precision timing accuracy down to parts in 10^{-10} using 1 second averaging and parts in 10^{-12} using 1000 second averaging. The on-board precision temperature-compensated oscillator and jitter reducer provide excellent phase-noise performance and above average holdover accuracy during loss of satellite lock conditions. Provision is made for an external reference input when a higher-performance clock is available. The CKM provides precision reference and one pulse-per-second inputs to the DE for data time stamping. It is expected that the TangerineSDR will be able to achieve ± 50 ns time-stamp accuracy on each sample. The CKM also provides up to 10 clock outputs from an on-board precision synthesizer. Each output can be set to an independent frequency and starting phase. These outputs drive the clock inputs to the DE, providing frequency agility to the TangerineSDR components (such as the RFMs).

3.3 RF Module

The RF Module, or RFM, is diagrammed in Figure 6. Each RFM is essentially a two-channel, high-speed, precision data acquisition board. The RFM takes signals from the two antenna inputs, digitizes them, and provides two high-speed (typically 122.88 MSPS) 14-bit data streams to the DE. This analog-to-digital converter (ADC) subsystem creates a dual-channel direct-sampling receiver capable of processing 100 kHz to 60 MHz of spectrum simultaneously. The inclusion of a noise source, multiple input attenuators, a low-noise amplifier, and support for custom filter options makes the RF module especially useful for many applications, including PSWS, radio astronomy, academic, and satellite work. The on-board noise source is electronically selectable with a switching time of < 15 ms, has an fixed excess noise ratio (ENR) close to 15 dB (9.6 kK). The noise source should be profiled against an external laboratory standard when used in high accuracy applications. The dual-channel architecture allows both input channels to be sampled synchronously. The DE has two RFM slots, providing up to four synchronously sampled inputs on one DE. Provisions are also made for synchronizing multiple DEs in order to provide even wider synchronous systems.

3.4 Open Architecture

All hardware and software for the TangerineSDR project is being released under open source hardware and software licenses. Hardware will be released under the TAPR Open Hardware License (TAPR OHL, `https://tapr.org/the-tapr-open-hardware-license/`), and software is being released on the GNU General Public License Version 3 (GPLv3, `https://www.gnu.org/licenses/gpl-3.0.en.html`). This will allow for customization and development that will enable many use cases for the TangerineSDR beyond the PSWS.

Even without hardware modification, this openness allows for significant flexibility. For instance, custom FPGA loads can be independently developed for radio astronomy, academic, and specialized custom applications. This allows users to maximize the available FPGA processing power by implementing only the signal processing algorithms actually required. Similarly, the user will have uninhibited access to CKM configuration. The user can use PC-based software to define the output frequencies and other characteristics of the synthesizer and upload that configuration to the CKM. The GPS configuration is also accessible to the user.

4 TangerineSDR and Radio JOVE

To illustrate one potential application of the TangerineSDR to radio astronomy, we present selected spectrograph observations from the Radio JOVE project. Radio JOVE is a NASA-supported citizen science and education/public outreach radio astronomy project started in 1998 to study radio emissions from Jupiter and the Sun (`https://radiojove.gsfc.nasa.gov/`; Arnold, 2014). This is a particularly relevant use case for the TangerineSDR, as plasma processes within Jupiter's magnetosphere naturally produce radio emissions with frequencies from approximately 3 to 40 MHz (Burke and Franklin, 1955; Zarka et al., 2001; Alexander et al., 1981; Clarke et al., 2014). These emissions, known as Jovian decametric emission due to having wavelengths tens of meters long, are all within the frequency range of the current TangerineSDR RFM design.

While the standard Radio JOVE system is capable of receiving a single narrow band signal at 20.1 MHz, advanced users often wish to observe a wide slice of spectrum which allows a significantly greater insight to physical processes. This prompted Richard Flagg, Jim Sky, and Dave Typinski to develop the Dual Polarization Spectrograph (DPS) (Typinski, 2014). The DPS consists of two swept-frequency receivers sharing a single local oscillator that sweeps 300 channels from 32 MHz to down to 16 MHz at a rate of 6.7 sweeps per second. Each channel has 30 kHz bandwidth. Each receiver has a 12-bit analog-to-digital converter, dynamic range of 50 dB, and noise figure (NF) of 7 dB (1.2 kK). This NF is insignificant compared to the galactic background of 100 kK at 15 MHz and 18 kK at 30 MHz. The antenna system developed for use with the DPS is an array of eight terminated folded-dipole elements that provides separate outputs for right- and left-hand circular polarization.

Figure 7 presents a 24 hr spectrogram measured at the AJ4CO Observatory in High Springs, Florida on 28 January 2014. The upper portion of the HF band is chosen because the terrestrial ionosphere typically shields out signals from space below approximately 10 MHz. This particular day was chosen because there is an instance of almost every kind of HF emission signature in this image. Jovian (Jupiter) non-Io-A emissions are observed as a triangular signature from 17 to 25 MHz around 0300 UT. Propagation “teepees”, which are believed to be HF band signatures of lightning (Fung et al., 2020), are observed above 26 MHz around 1530 UT and 2230 UT. Solar Type III radio emissions (Reid and Ratcliffe, 2014) are observed around 1500 UT, and an X-ray flare radio blackout (Benson, 1964; Frissell et al., 2014, 2019) is observed around 2000 UT. In addition to these natural signals, man-made signals such as receiver overloading (0030 and 1200 UT) and broadcast/communications channels (narrowband signals that extend for long periods of time) are also apparent.

We also present spectrograph observations of two types of Jovian emissions of particular interest: Figure 8 shows Jovian-L (long) bursts, while Figure 9 shows Jovian-S (short) bursts. Jovian-L bursts, as shown in Figure 8, typically consist of Gaussian noise with an intensity periodicity of 2 to 10 s (Carr and Reyes, 1999). The longer period, more vertical lanes are a combination of the natural variation in the emission source and scintillation due to propagation through the terrestrial ionosphere. The diagonal lanes modulating the L bursts in Figure 8 are thought to be produced by propagation through density variations within the Io plasma torus, a large ring of plasma around Jupiter consisting mostly of ionized volcanic gasses from the moon Io (Imai et al., 1992). The spectrogram shown in Figure 8 was made using the same DPS spectrograph used for Figure 7.

Figure 9 shows the signatures of Jovian-S bursts, which, unlike L bursts, have a sharply defined spectral structure. S bursts typically appear for intervals of a few seconds with a repetition rate of 2 to 400 s^{-1}, most commonly 20 s^{-1}. Individual bursts typically have a negative frequency drift rate on the order of -20 MHz s^{-1} (Carr and Reyes, 1999). Due to the high repetition rate and well-defined spectral structure, a high temporal cadence is a requirement for proper observation of S bursts. The top spectrogram in Figure 9 was made using the same DPS spectrograph used for Figures 7 and 8. While the S-bursts can be observed, they are undersampled and cannot be fully resolved. By contrast, the bottom spectrogram of Figure 9 shows measurements taken by a Tunable Wideband Receiver (TWB), an SDR instrument with a 2 MHz bandwidth capable of resolving spectrum at a 205 μs cadence for 250 ms at a time (Typinski et al., 2014). Although the capabilities of the TWB are limited in bandwidth and duration, the spectral structure of the S bursts is now well-resolved.

All of the observational examples presented here would benefit greatly from an SDR such as the TangerineSDR, which will be able to record 20 to 30 MHz of bandwidth continuously, rather than being required to sweep at a low rate across the HF band or be limited to to a relatively narrow bandwidth and short recording duration. A major advantage of an SDR-based spectrograph over a swept-frequency instrument is that the SDR has 100% integration time because its Discrete Fourier Transform (DFT) effectively samples every frequency channel simultaneously. Compared to the DPS instrument described above, an SDR having the same noise figure ($\sim$7 dB), channel bandwidth ($\sim$50 kHz), and temporal resolution ($\sim$150 ms) would produce spectrograms with around 10 dB greater signal to noise ratio. This would allow a much clearer picture of the Jovian emissions shown in Figures 7, 8, and 9 to be produced.

5 TangerineSDR Considerations for Radio Astronomy Applications

The observations of Section 4 illustrate the key requirements needed for many radio astronomy systems: a highly stable clock, precision timestamping, ability to collect phase-locked measurements from multiple antennas, the ability to make calibrated measurements of the amplitudes of received signals and noise, and facility for processing and transporting wideband data. The Radio JOVE Spectrograph Users Group (SUG) has produced a list of desired specifications for a new software defined radio (SDR) to support their operations (Dodd et al., 2019). Although this list of specifications is targeted to the Radio JOVE project, many aspects are applicable to radio astronomy at large. It should be recognized that this list is not meant to be a strict set of minimum requirements, but rather guidelines for what would make an excellent instrument for HF band radio astronomy. In this section, we highlight how key features of the TangerineSDR, whose architecture is described in Section 3, relate to Radio JOVE and radio astronomy in general.

Clock stability and precision timestamping requirements are handled by the Clock Module (CKM), described in Section 3.2. The GPSDO-based CKM ensures that the entire TangerineSDR system maintains a frequency accuracy to within parts in 10^{-10} (using 1 second averaging), and that provisions are made to achieve ± 50 ns timestamp accuracy for each data sample. While this level of precision will not allow for Very Large Baseline Interferometry (VLBI), which typically requires active hydrogen maser clocks costing approximately US$250,000, it will allow for applications such as the comparison of Jovian S-burst time of arrival observed at distant stations. Each TangerineSDR clock module can both output and accept external clock signals, allowing the use of superior clocks (if available) and physically synchronizing arrays of multiple TangerineSDRs for applications such as interferometry and electronic beamforming.

The requirement for the ability to collect phase-locked measurements from multiple antennas is addressed by the RF module (RFM, described in Section 3.3), the data engine (DE, described in Section 3.1), and the CKM. Each HF RFM has two antenna inputs corresponding to two phase-locked independent receive channels, allowing for polarization measurements using a TangerineSDR with only a single RFM. Up to four independent, phase-locked channels can be supported by a single DE by adding a second RFM. Finally, the ability to synchronize multiple TangerineSDRs together using the CKM's ability to output and accept external clock signals allows for the implementation of complex, electronically steerable antenna array designs.

Radiometry, the field of measuring total RF noise power within a given bandwidth coming from within a given area of sky, is the key to radio astronomy. On the TangerineSDR, this is enabled by the on-board noise source on the RFM that can be profiled against an external reference. By placing the noise source at the antenna inputs ahead of all signal processing, it will be possible to calibrate signal and noise levels measured by the receiver. Assuming an array of inefficient terminated folded dipole (TFD) antenna elements and several dB of feed line loss, the 20 MHz galactic background at the receiver input connector is expected to be approximately 4 to 8 kK. Thus, the planned noise source excess noise ratio (ENR) of 15 dB (9.6 kK) will be sufficient for both calibrating the receiver and measuring receiver gain stability at realistic signal levels.

Facility for processing and transporting wideband data is afforded by the direct sampling receiver capable of processing 100 kHz to 60 MHz of spectrum simultaneously. These signals are passed directly to the FPGA, allowing for tremendous flexibility in how the data is processed. Ultimately, the output bandwidth of the TangerineSDR to external computers is limited by the gigabit Ethernet and USB 3.0 interfaces to 20 to 30 MHz. However, the ability to implement custom, on-FPGA processing and easily synchronize multiple TangerineSDRs mitigates this limitation. Additionally, Section 4 has demonstrated the scientific utility of 15 to 20 MHz of observable bandwidth.

As previously discussed, a key to the utility of the TangerineSDR platform is its open source nature in both hardware and software. While the software that is being developed for the HamSCI PSWS will be centered around space weather applications, it will include a "firehose" mode functionality that will stream raw data samples at maximum speed from the TangerineSDR to the computer of the user's choosing. This mode will satisfy the needs of many radio astronomers. For users with additional needs, provisions are being made to allow for customization of all software, including the FPGA images, as described in Section 3.4.

Finally, the modular, open hardware design allows potential extensibility of the TangerineSDR platform to applications beyond those using the 100 kHz – 60 MHz band. This can be achieved using the current RFM design with the addition of appropriate front end filters, low noise amplifier (LNA), and down-converter. The SDR could also function in undersampling mode (i.e., without a down-converter) provided the front end filters are of the quality required to do so. Alternatively, completely new RFMs could be designed and produced. Potential radio astronomy applications include pulsar detection in the VHF through microwave bands, the study of galactic neutral hydrogen clouds by using Doppler shift around 1.42 GHz to infer the galactic rotation curve to infer the presence of dark matter, and age of re-ionization neutral hydrogen observations around 70 MHz. This is the 1.42 GHz neutral hydrogen emission from the early universe; it is so old that it has been red-shifted to around 70 MHz the same way the 3,000 K black-body peak (ref. Planck's Law) cosmic microwave background radiation (CMBR) from the early universe has been red-shifted to the 2.7 K peak we observe today.

6 Summary

The Ham Radio Science Citizen Investigation (HamSCI) Personal Space Weather Station (PSWS) project is a citizen science initiative to develop a new modular set of ground-based instrumentation for the purpose of studying the structure and dynamics of the terrestrial ionosphere, as well as the larger, coupled geospace system. PSWS system instrumentation includes radio receivers sensitive to frequencies ranging from the very low frequency (VLF) through very high frequency (VHF) bands, a Global Navigation Satellite System (GNSS) receiver to provide Total Electron Content (TEC) measurements and serve as a precision time and frequency reference, and a ground magnetometer sensitive to ionospheric and geospace currents. Although the PSWS is designed primarily for space weather and space science, its modular and open design in both hardware and software allows for a variety of use cases.

The core radio instrument of the PSWS, the TangerineSDR, is a wideband, direct sampling 100 kHz to 60 MHz field programmable gate array (FPGA)-based software defined radio (SDR). This SDR has been designed from the ground up to account for key requirements needed by radio astronomy systems: a highly stable clock, precision timestamping, ability to collect phase-locked measurements from multiple antennas, the ability to make calibrated measurements of the amplitudes of received signals and noise, and facility for processing and transporting wideband data.

The initial design of the TangerineSDR makes it immediately usable for radio astronomy applications in the HF band, such as the study of Jovian Decametric Emissions. The wideband capability of the TangerineSDR makes it possible to capture the full spectral signatures of both Jovian L- and S- bursts, while the precision timestamping and high temporal resolution measurements will allow for accurate comparison of S-burst spectral structures observed from geographically distant locations. Through the use of downconverters, LNAs, and filters, it will be possible to use the TangerineSDR for radio astronomy applications at higher frequencies. The modular and open design makes the TangerineSDR highly extensible, and its target price of US$500-$1000 makes it affordable to amateur and professional scientists alike.

Acknowledgments Support for this work was provided by NSF Grants AGS-2002278, AGS-1932997, and AGS-1932972. The authors of this work are especially grateful for the HamSCI and amateur radio community volunteers who have contributed engineering, testing, and data collection efforts to the Personal Space Weather Station project. The paper includes results that were obtained using the HF propagation toolbox, PHaRLAP, created by Dr Manuel Cervera, Defence Science and Technology Group, Australia (manuel.cervera@dsto.defence.gov.au). This toolbox is available by request from its author. We are grateful for the use of the Free Open Source Software projects used in this analysis, including Ubuntu Linux, python (van Rossum, 1995), matplotlib (Hunter, 2007), Cartopy Met Office (2010), NumPy (Oliphant, 2007), SciPy (Jones et al., 2001), pandas (McKinney, 2010), xarray (Hoyer and Hamman, 2017), iPython (Pérez and Granger, 2007), and others (Millman and Aivazis, 2011).

References

J. K. Alexander, T. D. Carr, J. R. Thieman, J. J. Schauble, and A. C. Riddle. Synoptic observations of Jupiter's radio emissions: Average statistical properties observed by Voyager. *Journal of Geophysical Research: Space Physics*, 86(A10):8529–8545, 9 1981. doi: 10.1029/ja086ia10p08529. URL `http://dx.doi.org/10.1029/ja086ia10p08529`.

S. Arnold. The NASA Radio Jove Project. In *Getting Started in Radio Astronomy*, pages 135–167. Springer, New York, NY, 2014. doi: 10.1007/978-1-4614-8157-7_7. URL `http://dx.doi.org/10.1007/978-1-4614-8157-7_7`.

R. F. Benson. Electron collision frequency in the ionospheric D region. *Radio Science*, 68D(10):1123–1126, 10 1964. URL `https://nvlpubs.nist.gov/nistpubs/jres/68D/jresv68Dn10p1123_A1b.pdf`.

D. Bilitza, D. Altadill, V. Truhlik, V. Shubin, I. Galkin, B. Reinisch, and X. Huang. International Reference Ionosphere 2016: From ionospheric climate to real-time weather predictions. *Space Weather*, 15(2):418–429, 2 2017. ISSN 15427390. doi: 10.1002/2016SW001593. URL `http://dx.doi.org/10.1002/2016SW001593`.

B. F. Burke and K. L. Franklin. Observations of a variable radio source associated with the planet Jupiter. *Journal of Geophysical Research*, 60(2):213–217, 6 1955. doi: 10.1029/jz060i002p00213. URL `http://dx.doi.org/10.1029/jz060i002p00213`.

T. D. Carr and F. Reyes. Microstructure of Jovian decametric S bursts. *Journal of Geophysical Research: Space Physics*, 104(A11):25127–25141, 11 1999. ISSN 21699402. doi: 10.1029/1999ja900342. URL `http://dx.doi.org/10.1029/1999ja900342`.

M. A. Cervera and T. J. Harris. Modeling ionospheric disturbance features in quasi-vertically incident ionograms using 3-D magnetoionic ray tracing and atmospheric gravity waves. *Journal of Geophysical Research: Space Physics*, 119(1):431–440, 2014. doi: 10.1002/2013JA019247. URL `http://dx.doi.org/10.1002/2013JA019247`.

T. E. Clarke, C. A. Higgins, J. Skarda, K. Imai, M. Imai, F. Reyes, J. Thieman, T. Jaeger, H. Schmitt, N. P. Dalal, J. Dowell, S. W. Ellingson, B. Hicks, F. Schinzel, and G. B. Taylor. Probing Jovian decametric emission with the long wavelength array station 1. *Journal of Geophysical Research: Space Physics*, 119 (12):9508–9526, 12 2014. ISSN 21699402. doi: 10.1002/2014JA020289. URL `http://dx.doi.org/10.1002/2014JA020289`.

C. J. Coleman. A ray tracing formulation and its application to some problems in over-the-horizon radar. *Radio Science*, 33(4):1187–1197, 1998. ISSN 1944-799X. doi: 10.1029/98RS01523. URL `http://dx.doi.org/10.1029/98RS01523`.

K. Collins, D. Kazdan, and N. A. Frissell. Ham Radio Forms a Planet-Sized Space Weather Sensor Network. *Eos*, 102, 2 2021a. ISSN 0096-3941. doi: 10.1029/2021eo154389. URL `http://dx.doi.org/10.1029/2021eo154389`.

K. Collins, A. Montare, N. A. Frissell, and D. Kazdan. Citizen Scientists Conduct Distributed Doppler Measurement for Ionospheric Remote Sensing. *IEEE Geoscience and Remote Sensing Letters*, 2021b. ISSN 15580571. doi: 10.1109/LGRS.2021.3063361. URL `http://dx.doi.org/LGRS.2021.3063361`.

S. Cowling. Hands-On-SDR. *QEX*, (318):10–15, 1 2020. URL `http://www.arrl.org/qexhttps://hamsci.org/publications/hands-sdr-tangerinesdr`.

L. Dodd, R. S. Flagg, J. Sky, and D. Typinkski. Radio JOVE SUG SDR Design Specifications. Technical report, Radio JOVE Spectrograph Users Group (SUG), 10 2019. URL `http://www.radiojove.org/SUG/Pubs/Radio%20JOVE%20SUG%20SDR%20Design%20Specifications%202019%2010%2024,%20Dodd,%20et%20al.pdf`.

W. Engelke. TangerineSDR Database and Control System Architecture. In *2020 HamSCI Workshop*, Scranton, PA, 6 2020. HamSCI. URL `https://hamsci.org/publications/tangerinesdr-database-and-control-system-architecture`.

W. D. Engelke. TangerineSDR Software Demo. In *2021 HamSCI Workshop*, Scranton, PA (Virtual), 6 2021. HamSCI. URL `https://hamsci.org/publications/tangerinesdr-software-demo`.

N. A. Frissell, E. S. Miller, S. Kaeppler, F. Ceglia, D. Pascoe, N. Sinanis, P. Smith, R. Williams, and A. Shovkoplyas. Ionospheric Sounding Using Real-Time Amateur Radio Reporting Networks. *Space Weather*, 12(12), 2014. ISSN 1542-7390. doi: 10.1002/2014SW001132. URL `http://dx.doi.org/10.1002/2014SW001132`.

N. A. Frissell, J. D. Katz, S. W. Gunning, J. S. Vega, A. J. Gerrard, G. D. Earle, M. L. Moses, M. L. West, J. D. Huba, P. J. Erickson, E. S. Miller, R. B. Gerzoff, W. Liles, and H. W. Silver. Modeling Amateur Radio Soundings of the Ionospheric Response to the 2017 Great American Eclipse. *Geophysical Research Letters*, 45(10):4665–4674, 5 2018. ISSN 19448007. doi: 10.1029/2018GL077324. URL `https://doi.org/10.1029/2018GL077324`.

N. A. Frissell, J. S. Vega, E. Markowitz, A. J. Gerrard, W. D. Engelke, P. J. Erickson, E. S. Miller, R. C. Luetzelschwab, and J. Bortnik. High-Frequency Communications Response to Solar Activity in September 2017 as Observed by Amateur Radio Networks. *Space Weather*, 17(1):118–132, 1 2019. ISSN 15427390. doi: 10.1029/2018SW002008. URL `http://dx.doi.org/10.1029/2018SW002008`.

S. F. Fung, D. Typinski, R. Flagg, T. Ashcraft, W. Greenman, C. Higgins, J. Brown, L. Dodd, F. Reyes, J. Sky, J. Thieman, and L. Garcia. Propagation Teepee: A Possible High-Frequency (15–30 MHz) Remote Lightning Signature Identified by Citizen Scientists. *Geophysical Research Letters*, 47(11):e2020GL087307, 6 2020. ISSN 19448007. doi: 10.1029/2020GL087307. URL `http://dx.doi.org/10.1029/2020GL087307`.

J. Gibbons, K. Collins, D. Kazdan, and N. Frissell. Grape Version 1: First Prototype of the Low-Cost Personal Space Weather Station Receiver. *HardwareX (Submitted)*, 2021.

S. Hoyer and J. Hamman. xarray: N-D labeled arrays and datasets in Python. *Journal of Open Research Software*, 5(1), 2017. doi: 10.5334/jors.148. URL `http://doi.org/10.5334/jors.148`.

J. D. Hunter. Matplotlib: A 2D graphics environment. *Computing In Science & Engineering*, 9(3):90–95, 2007. doi: 10.1109/MCSE.2007.55.

K. Imai, L. Wang, and T. D. Carr. A model for the production of Jupiter's decametric modulation lanes. *Geophysical Research Letters*, 19(9):953–956, 5 1992. ISSN 19448007. doi: 10.1029/92GL00942. URL `http://dx.doi.org/10.1029/92GL00942`.

E. Jones, T. Oliphant, P. Peterson, and others. SciPy: Open source scientific tools for Python, 2001. URL `http://www.scipy.org/`.

H. Kim, J. Madey, D. M. W. II, D. Larsen, S. H. Cowling, N. A. Frissell, and J. Weygand. Preliminary Data Analysis of PSWS Magnetometer Data. In *2021 HamSCI Workshop*, Scranton, PA (Virtual), 6 2021. HamSCI. URL `https://hamsci.org/publications/preliminary-data-analysis-psws-magnetometer-data`.

J. Madey, I. I. David Witten, H. Kim, D. Larsen, S. H. Cowling, and N. A. Frissell. PSWS Ground Magnetometer Hardware. In *2021 HamSCI Workshop*, Scranton, PA (Virtual), 6 2021. HamSCI. URL `https://hamsci.org/publications/psws-ground-magnetometer-hardware`.

W. McKinney. Data Structures for Statistical Computing in Python. In S. van der Walt and J. Millman, editors, *Proceedings of the 9th Python in Science Conference*, pages 51–56, 2010.

Met Office. Cartopy: a cartographic python library with a matplotlib interface, 2010. URL `http://scitools.org.uk/cartopy`.

K. J. Millman and M. Aivazis. Python for Scientists and Engineers. *Computing in Science & Engineering*, 13(2):9–12, 2011. doi: 10.1109/MCSE.2011.36. URL `http://dx.doi.org/10.1109/MCSE.2011.36`.

T. E. Oliphant. Python for Scientific Computing. *Computing in Science Engineering*, 9(3):10–20, 5 2007. ISSN 1521-9615. doi: 10.1109/MCSE.2007.58. URL `http://dx.doi.org/10.1109/MCSE.2007.58`.

F. Pérez and B. E. Granger. IPython: a System for Interactive Scientific Computing. *Computing in Science and Engineering*, 9(3):21–29, 5 2007. ISSN 1521-9615. doi: 10.1109/MCSE.2007.53. URL http://ipython.org.

H. A. S. Reid and H. Ratcliffe. A review of solar type III radio bursts, 7 2014. ISSN 16744527. URL http://dx.doi.org/10.1088/1674-4527/14/7/003.

J. Rizzo. VLF Module for Tangerine SDR Progress Update. In *2021 HamSCI Workshop*, Scranton, PA (Virtual), 6 2021. HamSCI. URL https://hamsci.org/publications/vlf-module-tangerine-sdr-progress-update.

D. Typinski. The Dual Polarization Spectrograph and the TFD Array. In *Radio JOVE Meeting*, Green Bank, WV, 7 2014. AJ4CO Observatory. URL http://www.typnet.net/AJ4CO/Publications/The%20DPS%20and%20TFD%20Array,%20Typinski%20(RJ,%202014)%20Sllides%20and%20Notes.pdf.

D. Typinski, R. Flagg, and W. Greenman. The Tunable Wideband Receiver. In *Radio JOVE Meeting*, Greenbank, WV, 7 2014. Radio JOVE. URL http://www.typnet.net/AJ4CO/Publications/The%20TWB,%20Typinski,%20Flagg,%20Greenman%20(RJ,%202014)%20Slides%20and%20Notes.pdf.

G. van Rossum. Python tutorial. Technical Report CS-R9526, Centrum voor Wiskunde en Informatica (CWI), Amsterdam, 5 1995.

P. Zarka, J. Queinnec, and F. J. Crary. Low-frequency limit of Jovian radio emissions and implications on source locations and Io plasma wake. *Planetary and Space Science*, 49(10-11):1137–1149, 8 2001. ISSN 00320633. doi: 10.1016/S0032-0633(01)00021-6. URL http://dx.doi.org/10.1016/S0032-0633(01)00021-6.

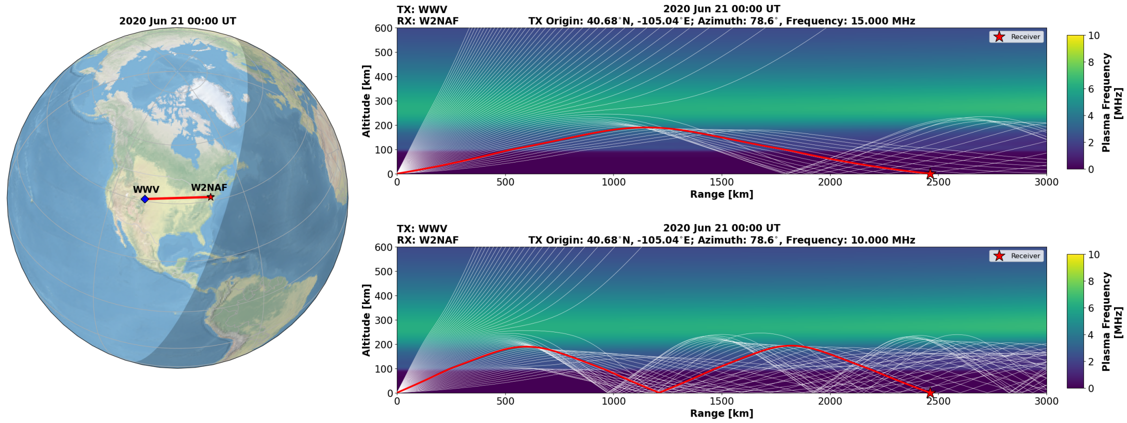

Figure 1: 2D numerical raytraces illustrating high frequency (HF) ionospheric refraction and radio wave propagation. The map on the left indicates the locations of the WWV transmitter near Fort Collins, Colorado (blue diamond) and the W2NAF receiver in Spring Brook Township, Pennsylvania (red star). The top raytrace shows computed ray paths for a 15 MHz radio wave along the WWV-W2NAF path, while the bottom shows paths for a 10 MHz wave. The red path indicates the ray that links the transmitter to the receiver. Both raytraces were computed using the PHaRLAP raytracing toolkit with the empirical International Reference Ionosphere 2016 (IRI2016) model.

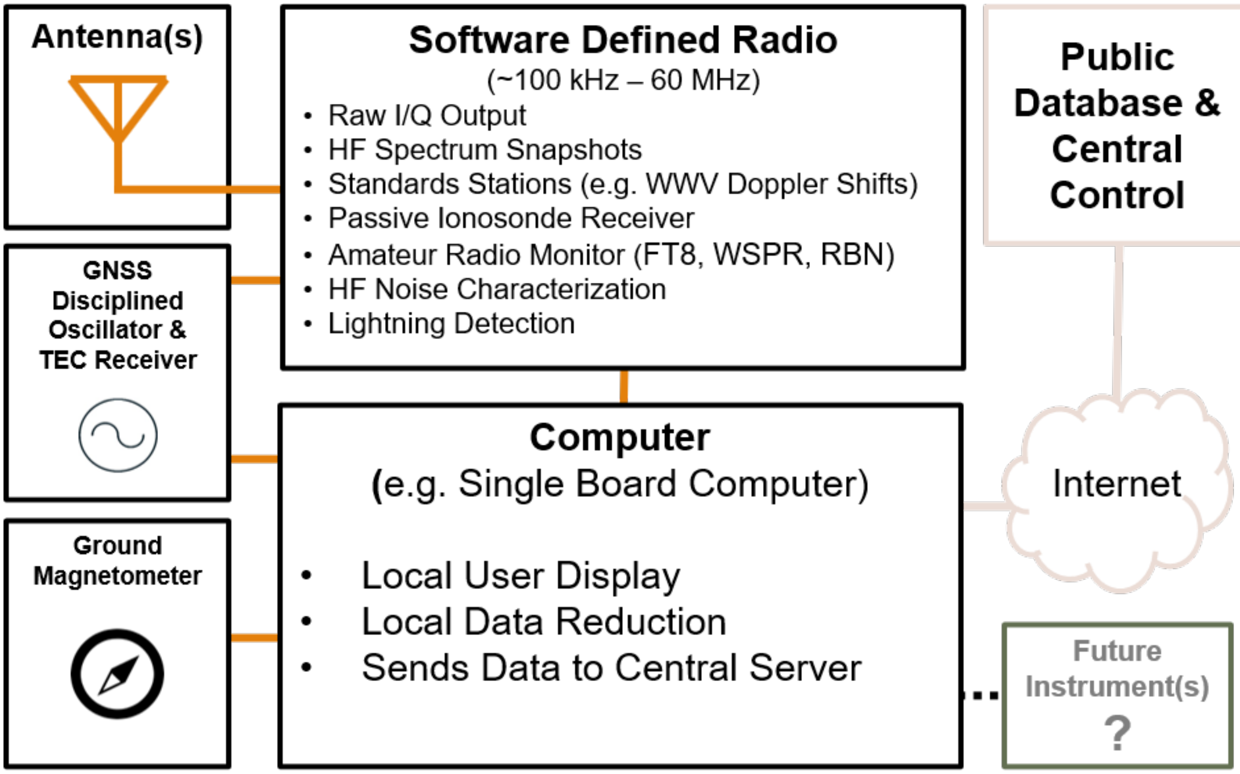

Figure 2: Block diagram of the HamSCI Personal Space Weather Station (PSWS). The three core instruments of the standard PSWS are the software defined radio (SDR), Global Navigation Satellite System (GNSS) receiver, and ground magnetometer. The GNSS receiver acts as both a precision frequency and time reference for the entire PSWS, as well an an ionospheric scintillation and total electron content (TEC) monitor. The TangerineSDR described in Section 3 will provide both the SDR and GNSS receiver functionality. A modular design allows for many variations in instrumentation.

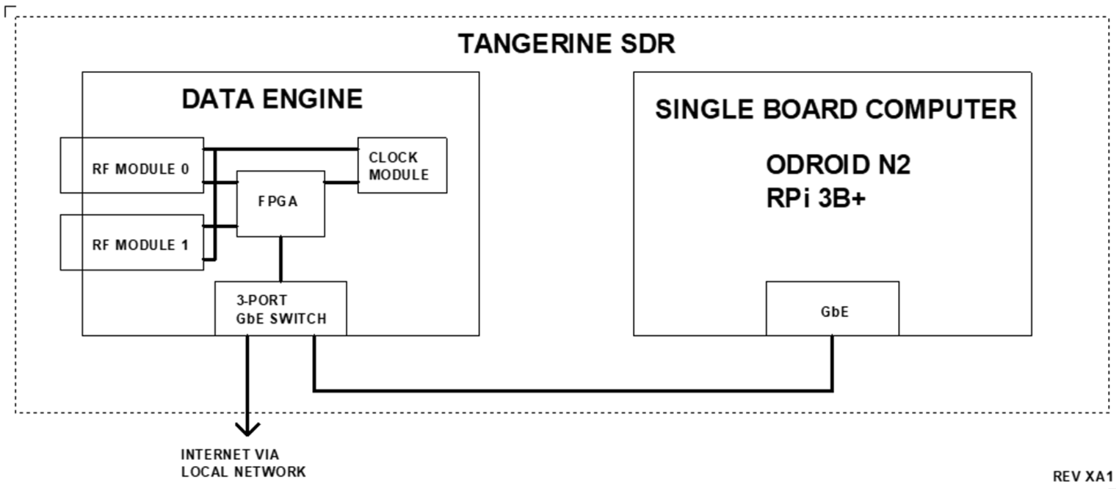

Figure 3: The TangerineSDR system consists of two main components. The component on the left consists of a three or four board modular stack consisting of a Data Engine (DE) carrier board, a Clock Module (CKM) and one or two RF Modules (RFM). On the right, a Single Board Computer (SBC) or other general-purpose computer acts as the host, providing networking, protocol formatting, and other functions.

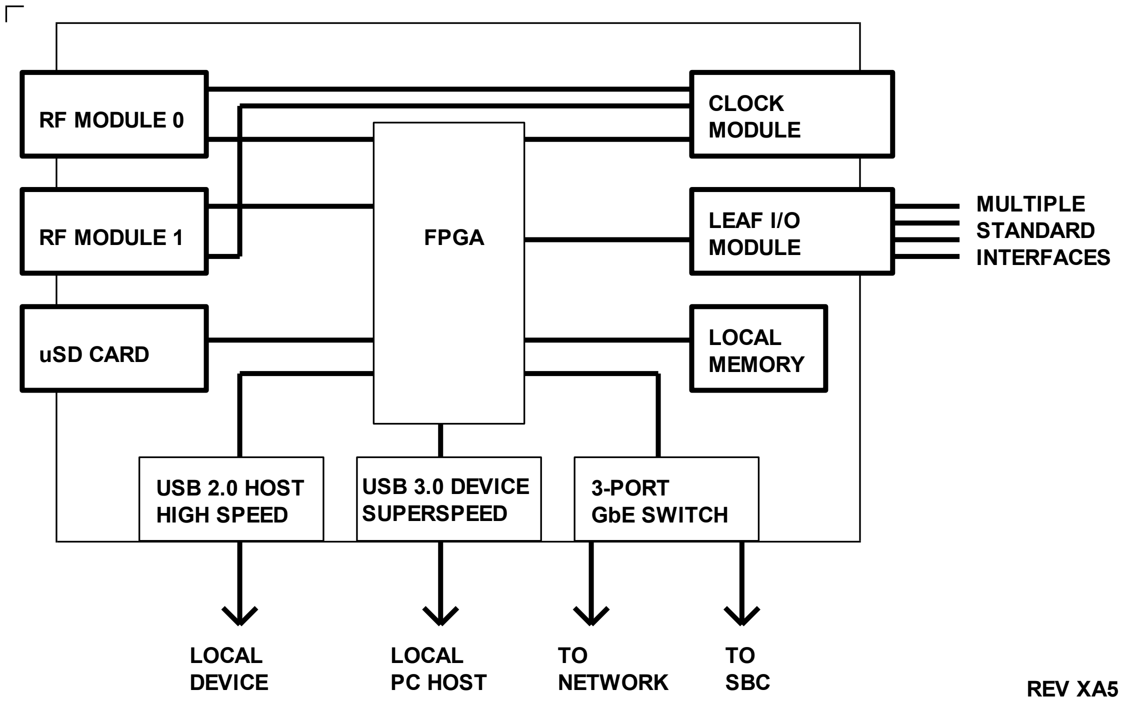

Figure 4: Block diagram of the TangerineSDR Data Engine (DE). The DE is the heart of the radio portion of the TangerineSDR and offers two sockets for RF Modules (RFM), a single socket for a Clock Module (CKM), and a low-speed LEAF interface. The Intel MAX10 FPGA is responsible for processing data produced by the RFMs, CKM, and LEAF instruments. Processed data is sent to other computers via USB or gigabit Ethernet.

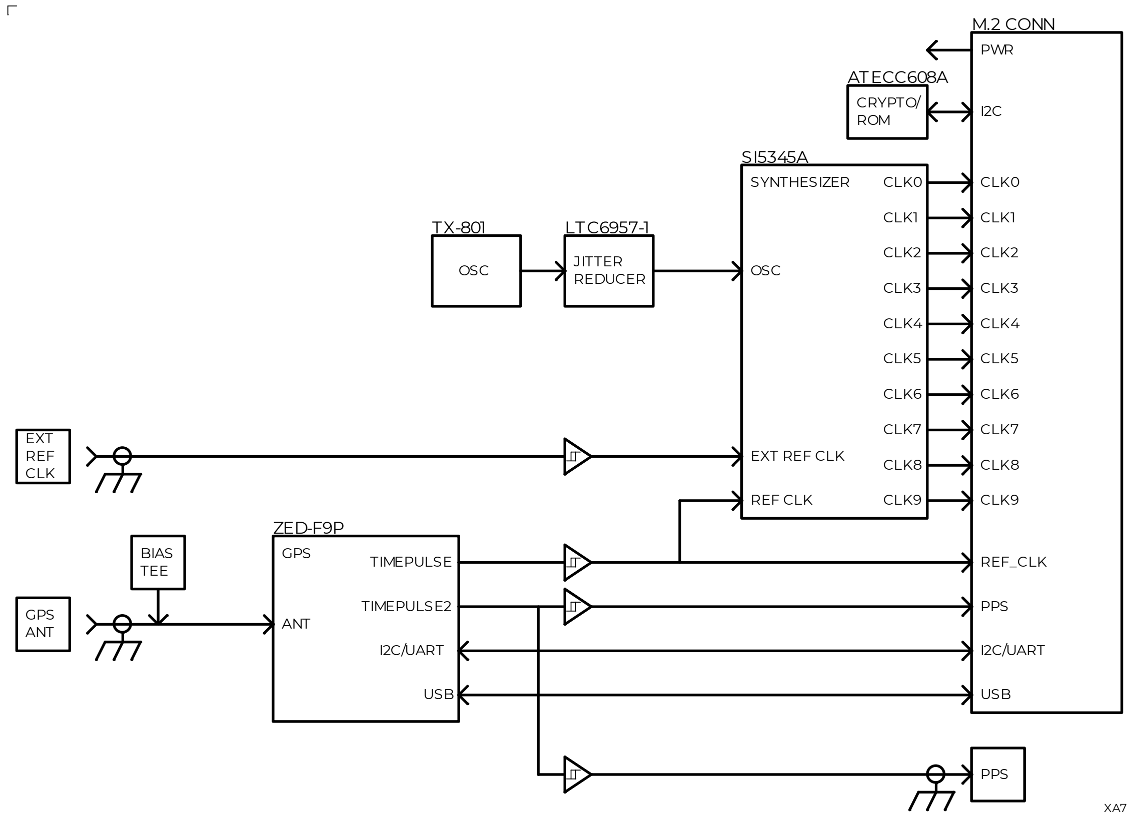

Figure 5: Block diagram of the TangerineSDR Clock Module (CKM). The CKM has an on-board multi-band Global Navigation Satellite System (GNSS) receiver enabling ionospheric total electron content (TEC) and scintillation measurements, as well as providing precision timing accuracy down to parts in 10^{-10} using 1 second averaging and parts in 10^{-12} using 1000 second averaging.

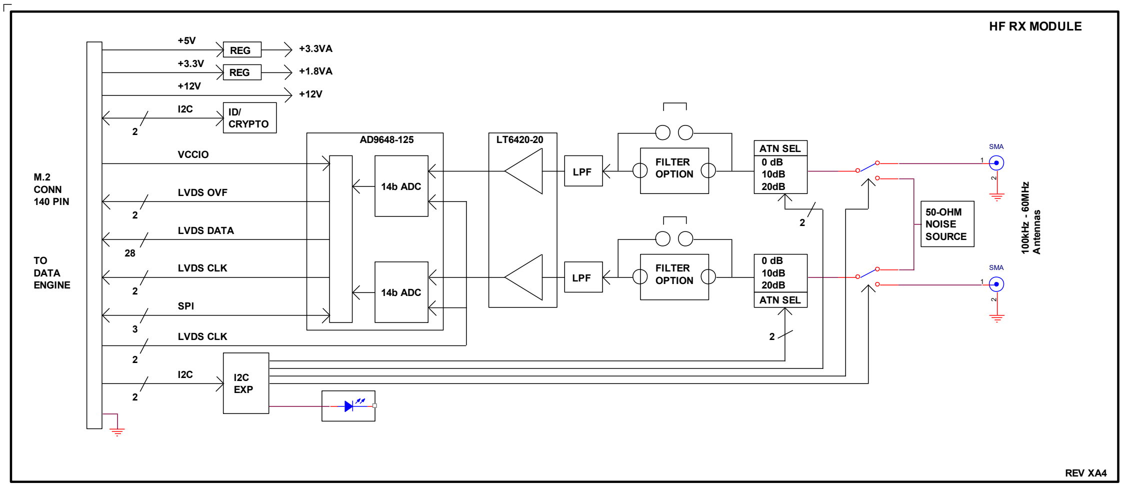

Figure 6: Block diagram of the TangerineSDR RF Module (RFM). Each RFM is a dual-channel direct-sampling receiver capable of processing 100 kHz to 60 MHz of spectrum simultaneously. Each Data Engine (DE) has two RFM slots, providing up to four synchronously sampled inputs on one DE. Provisions are also made for synchronizing multiple DEs in order to provide even wider synchronous systems.

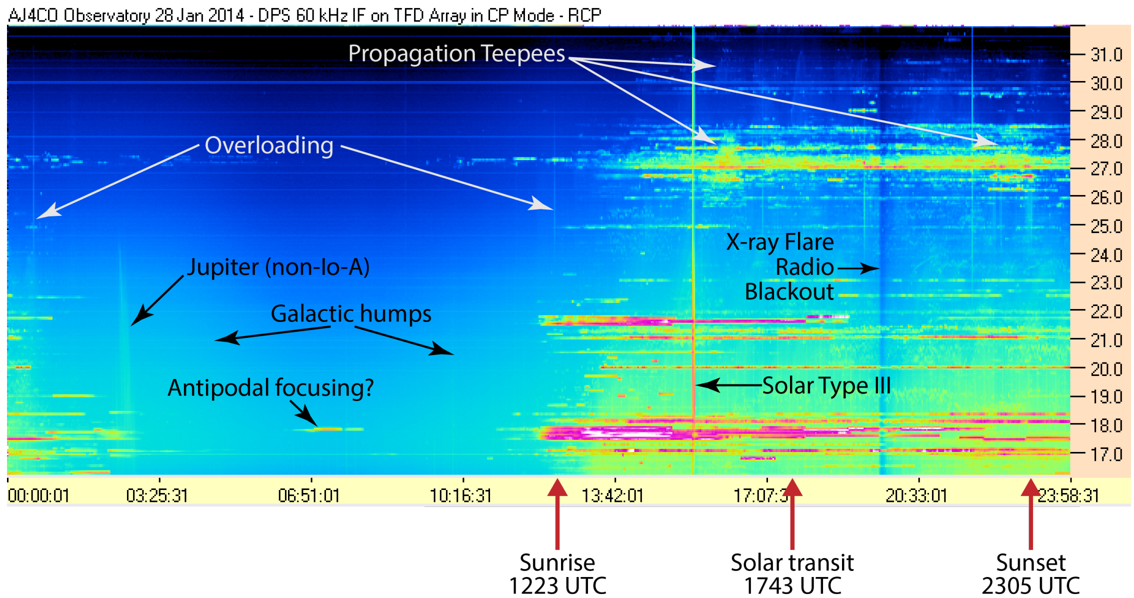

Figure 7: 24-hour spectrogram of the upper HF band. This spectrogram was produced using the Dual Polarization Spectrograph (DPS) designed by Richard Flagg, Jim Sky, and Dave Typinski. This particular day was chosen because there is an instance of almost every kind of HF emission signature in this image: Jupiter, solar, the galactic background, radar, and communications.

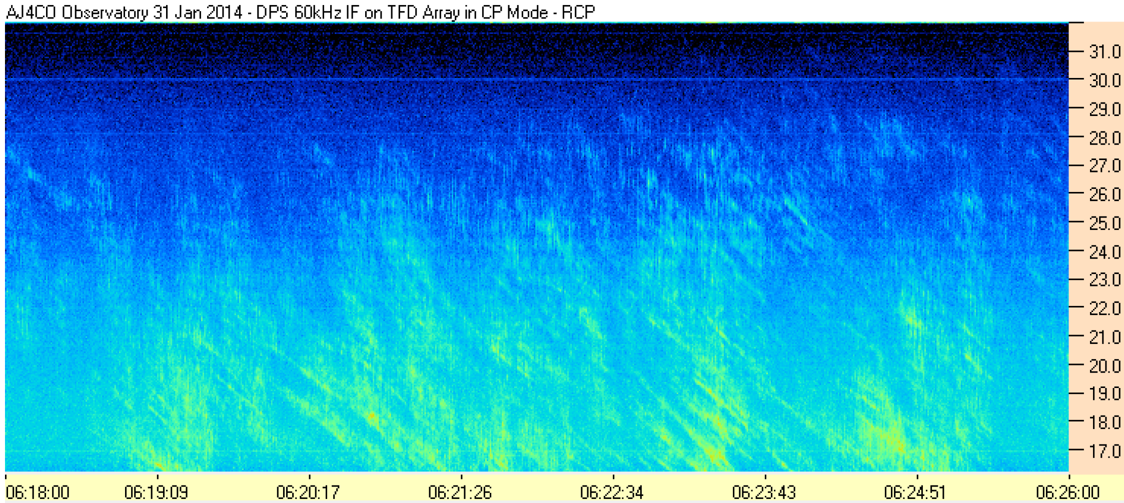

Figure 8: Jovian L-bursts. This spectrogram was produced using the same instrument as in Figure 7. The diagonal lanes are thought to be produced by propagation through density variations within the Io plasma torus, a large ring of plasma around Jupiter consisting mostly of ionized volcanic gasses from Io. The longer period, more vertical lanes are a combination of the natural variation in the emission source and scintillation due to propagation through the terrestrial ionosphere.

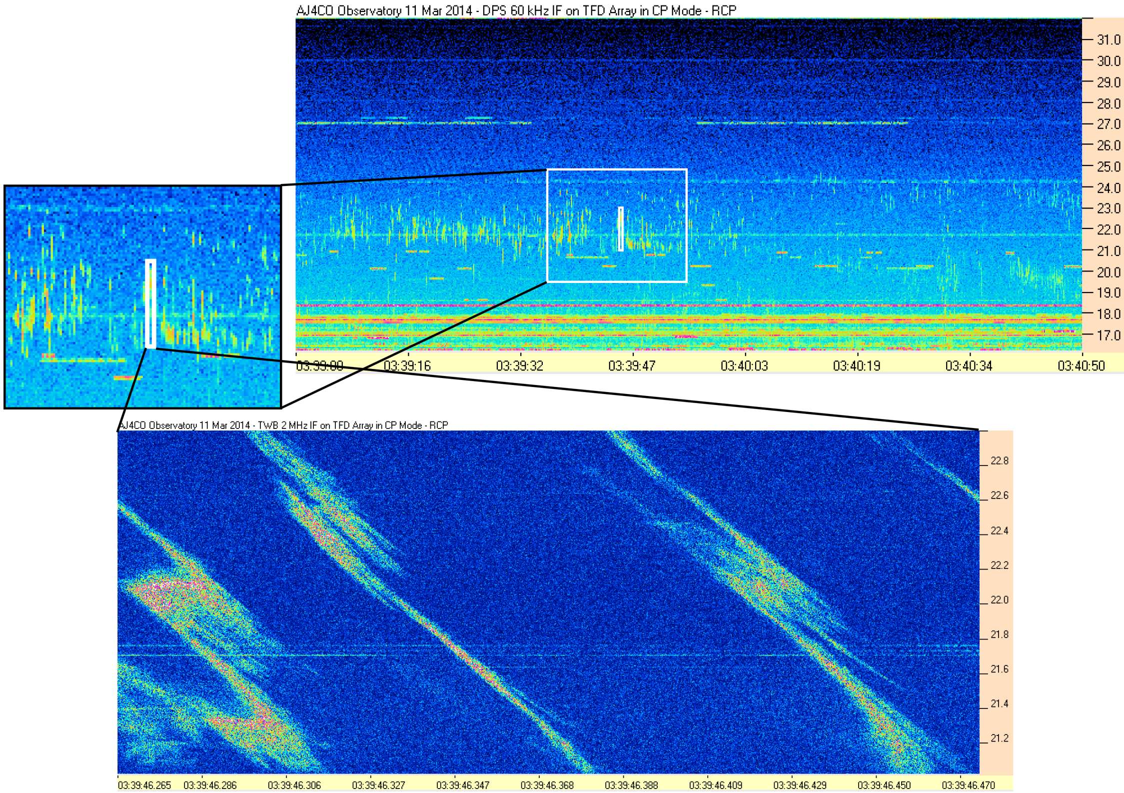

Figure 9: A comparison of Jovian S bursts as viewed by swept-frequency and SDR-based spectrographs. The top spectrogram was produced using the same instrument as in Figure 7. The lower spectrogram was produced using an SDR-based instrument designed and built by Richard Flagg, Wes Greenman, and Dave Typinski.